Chiral Guest Binding as a Probe of Macrocycle Dynamics and Tautomerism in a Conjugated Tetrapyrrole

ARTICLE *in* JOURNAL OF THE AMERICAN CHEMICAL SOCIETY · JANUARY 2014

Impact Factor: 12.11 · DOI: 10.1021/ja4124175 · Source: PubMed

7 AUTHORS, INCLUDING:

Jan Labuta
National Institute for Materials Science
30 PUBLICATIONS **376** CITATIONS
SEE PROFILE

Zdenek Futera
University College Dublin
16 PUBLICATIONS **92** CITATIONS
SEE PROFILE

Hana Kourilova
Charles University in Prague
8 PUBLICATIONS **73** CITATIONS
SEE PROFILE

Jonathan P Hill
National Institute for Materials Science
288 PUBLICATIONS **8,693** CITATIONS
SEE PROFILE

JACS
JOURNAL OF THE AMERICAN CHEMICAL SOCIETY
Article
pubs.acs.org/JACS

Chiral Guest Binding as a Probe of Macrocycle Dynamics and Tautomerism in a Conjugated Tetrapyrrole

Jan Labuta,*[,†] Zdenek Futera,[§,‡] Shinsuke Ishihara,[†] Hana Kouřilová,[#] Yoshitaka Tateyama,[†,‡] Katsuhiko Ariga,[†,‡] and Jonathan P. Hill*[,†,‡]

[†]World Premier International Research Center for Materials Nanoarchitectonics, National Institute for Materials Science, 1-1 Namiki, Tsukuba, Ibaraki 305-0044, Japan

[§]Faculty of Science and Technology, Keio University, 3-14-1 Hiyoshi, Kohoku-ku, Yokohama 223-8522, Japan

[#]Department of Macromolecular Physics, Faculty of Mathematics and Physics, Charles University in Prague, V Holešovičkách 2, 180 00 Prague 8, Czech Republic

[‡]CREST and PRESTO, Japan Science and Technology Agency (JST), 4-1-8 Honcho, Kawaguchi, Saitama 333-0012, Japan

Supporting Information

ABSTRACT: We report chiral guest binding as a probe of prototropic tautomerism and macrocyclic inversion in a highly conjugated tetrapyrrole studied using ^{1}H NMR spectroscopy in conjunction with mandelic acid as the chiral guest. Both tautomerism and macrocycle inversion can be influenced in a non-trivial way depending on temperature and the respective concentrations of tetrapyrrole host, chiral guest or water. Chirality of the interacting guest is the key feature since it permits separation and detailed observation of macrocyclic inversion and tautomerism. Based on this, a methodology was developed to identify and characterize the dynamic processes. Our observations suggest that yields of products (e.g., of asymmetric reactions) can be affected by reactivity of functional groups (in molecules undergoing tautomerism or inversion) by varying solution properties including reagent concentrations and impurities such as water. This work establishes a connection between the important chemical concepts of chirality, tautomerism, and macrocyclic dynamics.

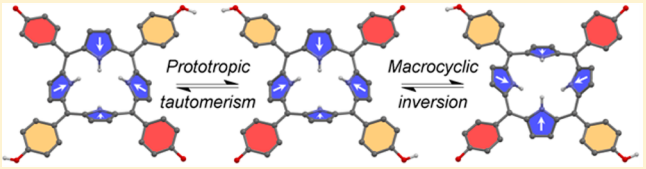

INTRODUCTION

Conjugated tetrapyrroles, especially porphyrins, have attracted a great deal of attention due to their ubiquity in nature. They are capable of adopting various tautomeric structures, and, although they are usually planar in form, they can be distorted into saddle-like non-planar forms by various means including protonation,[1−4] derivatization at β-[5] or *meso*-positions,[6] etc., giving them extra flexibility in their molecular structures. This property can be applied in several ways, for example, to sense enantiomeric purity,[4,7−9] to selectively detect anions,[10−12] or to determine water impurities in organic solvents.[13] Tetrapyrroles can also be utilized in colorimetric visualization of acid−base equilibria[14] or for naked-eye discrimination of methanol from ethanol.[15] Other possible uses of tetrapyrrole-like molecules as a memory based on transition between planar and saddle-like shapes[16] or as a chiral memory systems[9,17] have also been reported. Many other supramolecular concepts,[18] e.g. chiral amplification,[19,20] exploit specific features of tetrapyrrole macrocycles. Tautomerism and switching between planar- or saddle-like shapes of these compounds alters their physical (UV/vis, NMR, etc.) and chemical properties significantly making them available for specific sensing or derivatization purposes. However, analyses of these phenomena often neglect their dynamic aspects (macrocyclic inversion and tautomerism) which can significantly affect the operation of, for instance, sensing agents.

In this work, we describe the dynamics of prototropic phenol−hemiquinone tautomerism (a form of enol−keto tautomerism) and saddle-to-saddle macrocyclic inversion (ring-flip) in the diprotonated form of *meso*-tetrakis(3,5-di-*tert*-butyl-4-oxo-2,5-cyclohexadienylidene)porphyrinogen (**OxP**)[21−23] studied by using ^{1}H NMR spectroscopy[24,25] and theoretical modeling. This entailed in-depth study of the **OxP** system in conjunction with a chiral guest as a key feature for deconvolution of the complex dynamic behavior of the **OxP** macrocycle. A methodology was also developed to identify and characterize the dynamic processes.

Variations in the **OxP** structure upon protonation occur so that di-*tert*-butylated oxocyclohexadienylidene groups at *meso*-positions can reversibly interconvert with their phenol form (Figure 1). **OxP** possesses D_{2d} symmetry until diprotonation with mandelic acid **MA** (pK_a = 3.41) causes it to adopt D_2 symmetry and become chiral (Figure 1). Thus, $\mathbf{OxPH_2}^{2+}$ exists as two dynamically interchangeable enantiomers, (+)-$\mathbf{OxPH_2}^{2+}$ and (−)-$\mathbf{OxPH_2}^{2+}$.[26] Interchange from (+)- to (−)-$\mathbf{OxPH_2}^{2+}$ (or vice versa) is mediated by ring-flip or tautomerism (Figure

Received: December 6, 2013
Published: January 14, 2014

dx.doi.org/10.1021/ja4124175 | J. Am. Chem. Soc. 2014, 136, 2112−2118

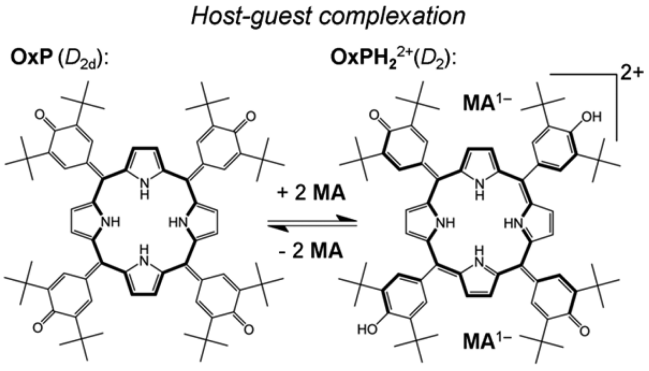

Figure 1. 1:2 host–guest complexation (diprotonation) process in the **OxP**/**MA** system and related reduction in symmetry.

2). In fact, there are certain similarities with known chiral memory systems[9,17] where interconversion between enantiomers is due to ring-flip only.

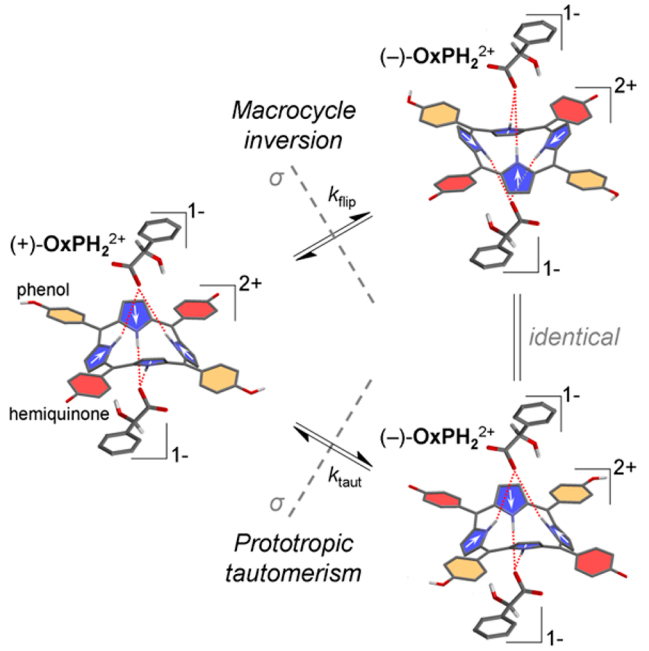

Figure 2. Dynamics of macrocyclic inversion (ring-flip) and prototropic tautomerism. Note that (−)-$\mathbf{OxPH_2}^{2+}$ structures on the right side are identical upon 90° rotation around axes perpendicular to the mean plane of $\mathbf{OxPH_2}^{2+}$.

RESULTS AND DISCUSSION

First, we investigated the strength of the acid–base interactions (at various temperatures) in the 1:2 host–guest $\mathbf{OxPH_2}^{2+}\cdot\mathbf{2MA}^-$ complex by using ^{1}H NMR titration experiments (for example, see Figure 3a). The $\mathbf{OxPH_2}^{2+}\cdot\mathbf{2MA}^-$ complex is formed through hydrogen bonding between the host's pyrrolic NH groups and the guest's COO^- group (as shown in Figure 2). ^{1}H NMR spectra were carefully fitted on the basis of spin exchange models (see Methods in Supporting Information (SI)) in order to separate resonances due to unprotonated and diprotonated forms of **OxP** (e.g., Figure 3b). In Figure 3a it can be seen, that during titration, resonances due to the complexed $\mathbf{OxPH_2}^{2+}$ form appear (full symbols in Figure 3a) and their intensity increases compared to those from uncomplexed **OxP**

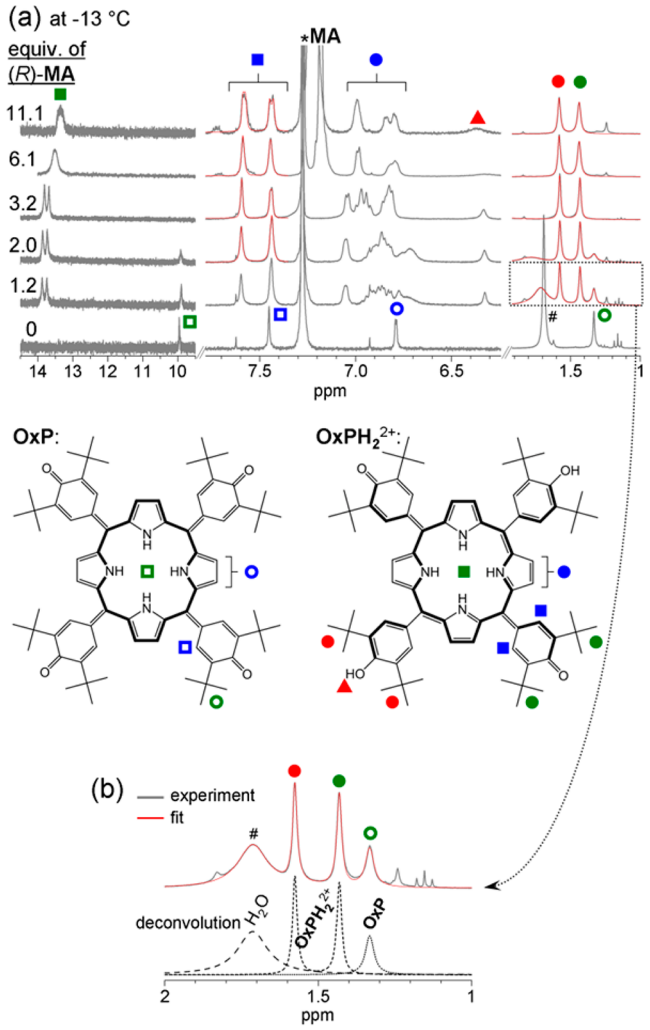

Figure 3. ^{1}H NMR investigation of acid–base interactions in 1:2 host–guest $\mathbf{OxPH_2}^{2+}\cdot\mathbf{2MA}^-$ complex. (a) Example of ^{1}H NMR spectra (gray = measured spectra, red = fitted spectra) at constant temperature (−13 °C) during titration of **OxP** (1.5 mM, chloroform-*d*, ca. 23 equiv of **W**) with (*R*)-**MA** (number of equivalents is indicated at each spectrum). Asterisk (*) and hash mark (#) denote residual chloroform and **W**, respectively. Spectral assignment to **OxP** and $\mathbf{OxPH_2}^{2+}$ structure, respectively, is shown under spectra. (b) Magnified region illustrating deconvolution of the spectrum into its components.

(empty symbols in Figure 3a). New pyrrolic NH resonance around 13.8 ppm and the phenolic OH resonance at 6.3 ppm due to $\mathbf{OxPH_2}^{2+}$ appear. Their broadening when more than 2 equiv of **MA** has been added is related to the chemical exchange of NH and OH protons of $\mathbf{OxPH_2}^{2+}$ with carboxylic protons of **MA**. In order to deduce the fraction of diprotonated **OxP** ($\mathbf{OxPH_2}^{2+}$), $f = [\mathbf{OxPH_2}^{2+}]/([\mathbf{OxP}] + [\mathbf{OxPH_2}^{2+}])$ ([ ] denotes equilibrium concentration, which is proportional to integrated intensity), the integrated intensities of **OxP** and $\mathbf{OxPH_2}^{2+}$ resonances were evaluated. In some cases certain resonances could not be observed (Figure 5b, pyrrolic NH resonance around 13.8 ppm and phenolic OH at 6.3 ppm) due to fast exchange at high (50 °C) temperature. However, in all cases deconvolution of *tert*-butyl resonances of the **OxP** spectra at 1.7–1.3 ppm could be performed (Figure 3b). In order to determine the strength of acid–base interaction the fraction *f* of $\mathbf{OxPH_2}^{2+}$ obtained by measurement was fitted using a 1:2 binding model (for one example of such fitting see Figure 4a).

dx.doi.org/10.1021/ja4124175 | J. Am. Chem. Soc. 2014, 136, 2112–2118

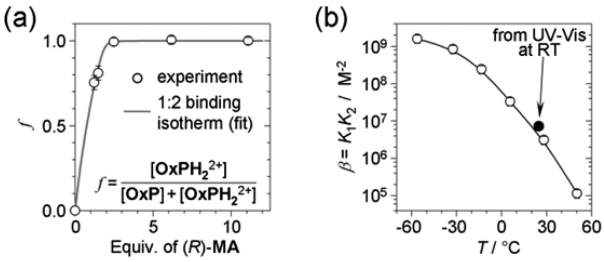

Figure 4. (a) Example of plot of fraction of diprotonated **OxP**, *f*, as obtained from titration experiment at −13 °C. Gray curve represents fit of 1:2 binding isotherm. (b) Temperature dependency of overall binding constant, β, as obtained in experiments similar to those in (a) at various temperatures. Full circle denotes value of β obtained from UV/vis at 25 °C.[7]

The 1:2 binding model was chosen on the basis of a previous UV/vis study[7] and also on the integrated intensity of phenolic OH resonances of diprotonated **OxP** being 2, which clearly supports 1:2 stoichiometry. Since the monoprotonated form of **OxP** cannot be directly observed by ^{1}H NMR (similar to the system in ref 4), only an overall binding constant, $\beta = K_1K_2$, can be obtained from a 1:2 host−guest binding model (for its derivation see Methods in SI). As expected, binding constant β increases with decreasing temperature as seen in Figure 4b. The lower boundary of binding cooperativity,[27] $\alpha = 4K_2/K_1$, was estimated from analysis of NMR binding isotherms to be $\alpha >$ 25 (at 28 °C; for α at other temperatures see Figure S1). This relatively high value of α is consistent with a low stability of the monoprotonated form[4,28] of **OxP**.

Splitting of some **OxP** resonances (hemiquinonoid *ortho*-H at 7.6−7.4 ppm and pyrrolic β-H at 7.1−6.8 ppm in e.g. Figure 3a at 11.1 equiv or Figure 5b at 26 equiv) is due to interaction with enantiopure (*R*)- or (*S*)-**MA** guest (for spectra with (*rac*)-**MA** see Figure S2). The induced non-equivalence is a result of D_2-symmetry breaking of the $\mathbf{OxPH_2}^{2+}$ host molecule upon binding a chiral guest. This gives rise to diastereotopic protons within the structure of $\mathbf{OxPH_2}^{2+}$ which are the basis of an enantiomeric excess (ee) detection method.[4,7,8] In the current study a chiral guest (**MA**) was used as a probe to investigate specifically the ring-flip processes.

Both tautomerism and ring-flip possess interesting non-trivial dependencies on parameters such as temperature or concentrations of **OxP**, **MA** and water (**W**). Temperature dependency of ^{1}H NMR spectra of **OxP** in the presence of (*R*)-**MA** is shown in Figure 5a. At 6.1 equiv of (*R*)-**MA** effectively all **OxP** molecules are diprotonated for the entire temperature range studied. Free and monoprotonated forms are not observable (are present at negligible concentrations) when 6.1 equiv of (*R*)-**MA** is used. This is due to the host−guest binding mechanism (for more details see section 1.2 in Methods in SI). There are several notable spectral features connected with the dynamic behavior of **OxP**. Over the temperature range studied it appears that fast exchange (on the NMR time scale) occurs between **MA** counterions (with **MA** in bulk) at the two binding sites of **OxP**, while **OxP** is maintained in a doubly protonated state. This is supported by variable temperature ^{1}H NMR measurements of **OxP** with (*rac*)-**MA** where a single resonance (e.g., that due to hemiquinonoid *ortho*-H) can be observed at depressed temperatures (see Figure S2). The pyrrolic NH peak around 13.2 ppm (Figure 5a) splits into two resonances at low temperature and, during heating, these merge and eventually broaden due to fast exchange of protons between $\mathbf{OxPH_2}^{2+}$ and

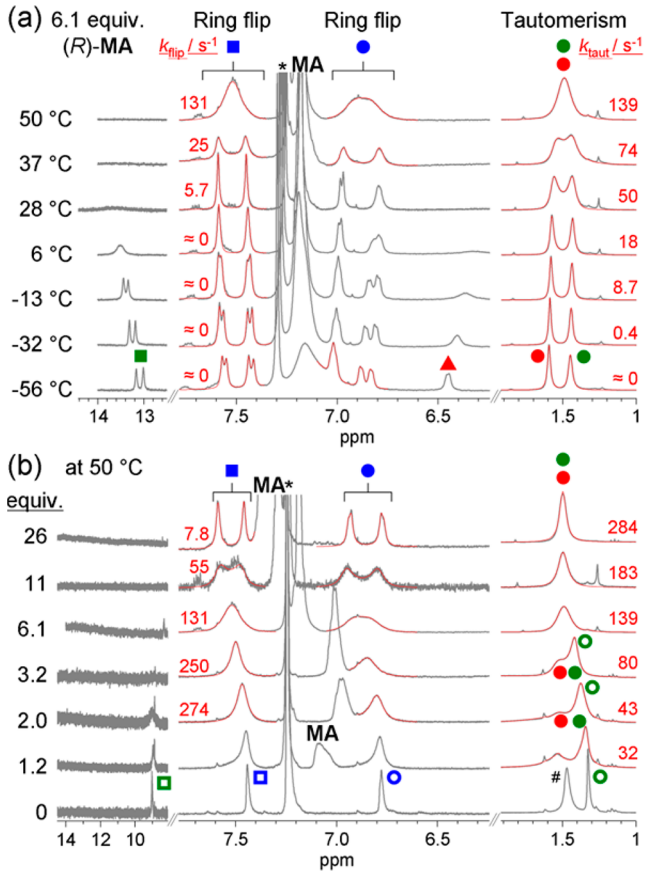

Figure 5. ^{1}H NMR spectral manifestation of prototropic phenol−hemiquinone tautomerism and saddle-to-saddle macrocyclic inversion (ring-flip) during (a) variable-temperature (VT) measurement and (b) titration experiment. (a) VT ^{1}H NMR of **OxP** (2.1 mM, chloroform-*d*, 15 equiv of **W**) with 6.1 equiv (*R*)-**MA**. (b) Titration of **OxP** (1.8 mM, chloroform-*d*, ca. 20 equiv of **W**) with (*R*)-**MA** at 50 °C (gray = measured spectra, red = fitted spectra; hash mark denotes **W**). For resonance assignment see Figure 3a.

(*R*)-$\mathbf{MA}^-$. The magnitude of splitting is related to the enantiomeric excess (ee) of **MA** (see Figure S3). At low temperature (e.g., spectrum at −56 °C in Figure 5a), additional splittings of the pyrrolic NH, hemiquinonoid *ortho*-H, and pyrollic β-H are a result of inhibited tautomerization and ring-flip in $\mathbf{OxPH_2}^{2+}$ which will be discussed in detail below. The phenolic OH resonance around 6.4 ppm also broadens with increasing temperature due to fast exchange of protons. The spectral manifestation of prototropic phenol−hemiquinone tautomerism is best illustrated by considering the *tert*-butyl part of the spectrum of **OxP** from 1.7 to 1.3 ppm. Spectra show two distinct resonances which coalesce with increasing temperature indicating that the tautomerism rate constant k_{taut} increases. The *tert*-butyl phenol−hemiquinone (around 1.5 ppm) and hemiquinonoid *ortho*-H (around 7.5 ppm) regions of the spectrum were fitted as a two-site symmetrical (non-*J*-interacting) exchange spin system $S_{\text{non-int-sym}}(\omega)$ using eq 1,[29]

$$S_{\text{non-int-sym}}(\omega) = M_0 \frac{2k + \alpha_A + \alpha_B}{\alpha_A\alpha_B - k^2}$$

$$\alpha_A = R_{2A} + k - i(\omega - \omega_A)$$

$$\alpha_B = R_{2B} + k - i(\omega - \omega_B) \quad (1)$$

dx.doi.org/10.1021/ja4124175 | J. Am. Chem. Soc. 2014, 136, 2112−2118

where M_0 is equilibrium magnetization, k (in s^{-1}) is rate constant of exchange, R_{2A} and R_{2B} (in s^{-1}) are spin−spin relaxation rates of each state, ω_A and ω_B (in rad s^{-1}) are resonance frequencies of each state when no exchange is present (k = 0 s^{-1}), ω (in rad s^{-1}) is an independent variable, and i is the unit imaginary number. For extraction and fitting of the absorption part of eq 1, see Methods in SI.

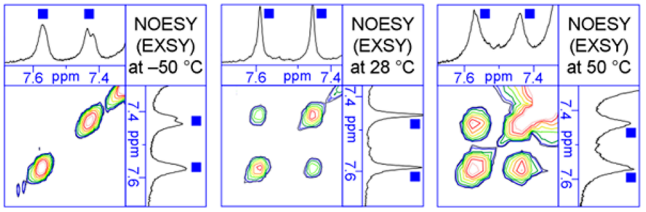

Figure 6. Partial 2D EXSY spectra (mixing time 500 ms) of hemiquinonoid *ortho*-H region of **OxP** (1.9 mM, chloroform-*d*, ca. 18 equiv of **W**) with ca. 16 equiv of (*R*)-**MA** proving ring-flip and its rate dependence on temperature. For resonance assignment see Figure 3a.

DFT calculations indicate that phenols of diprotonated **OxP** are predominantly at "trans" positions (i.e., at tetrapyrrole 5,15 positions as shown in Figure 1). The difference in free energies between cis and trans conformations is 3.5 kcal/mol at 25 °C, which corresponds to the presence of only 0.3% of the cis form. Therefore, diprotonated **OxP** adopts a predominantly trans form (as seen in Figure 1) with the cis form being a transition state. Exponential dependencies of k_{taut} on temperature (for various **MA** concentrations) can be seen in Figure 7a (top panel). Figure 7b shows dependencies of k_{taut} on **MA** concentration (at various temperatures). k_{taut} increases with increasing [**MA**] toward saturation indicating that **MA** anions actively participate in the tautomeric processes of **OxP** as proton carriers. Hemiquinonoid *ortho*-H and pyrrolic β-H regions of ^{1}H NMR spectra (e.g., Figure 5a) also contain information regarding the rate of ring-flip, characterized by the rate constant k_{flip}. The pyrrolic β-H region (around 6.9 ppm) of the spectrum was fitted as a two-site symmetrical (*J*-interacting) exchange spin system $S_{int\text{-}sym}(\omega)$ using eq 2,[30]

$$S_{int\text{-}sym}(\omega) = M_0\left(\frac{1-(J/2-ik)/A_-}{\omega-\omega_0+J/2-ik-iR_2+A_-} + \frac{1+(J/2-ik)/A_-}{\omega-\omega_0+J/2-ik-iR_2-A_-} + \frac{1+(J/2+ik)/A_+}{\omega-\omega_0-J/2+ik-iR_2+A_+} + \frac{1-(J/2+ik)/A_+}{\omega-\omega_0-J/2+ik-iR_2-A_+}\right)$$
$$A_\pm = [Q^2+(J/2\pm ik)^2]^{1/2} \quad (2)$$

where M_0 is equilibrium magnetization, k ($=k_{flip}$, in s^{-1}) is the rate constant of exchange, R_2 (in s^{-1}) is the spin−spin relaxation rate of both states, ω_0 (in rad s^{-1}) is the resonance frequency of the center of the spectral quartet, ω (in rad s^{-1}) is an independent variable, J (in Hz) is vicinal scalar coupling constant between spins, 2Q (in rad s^{-1}) is the difference in chemical shift between the true resonance frequencies of spins (when no exchange is present, k = 0 s^{-1}), and i is the unit imaginary number. For extraction and fitting of the absorption part of eq 2, see Methods in SI.

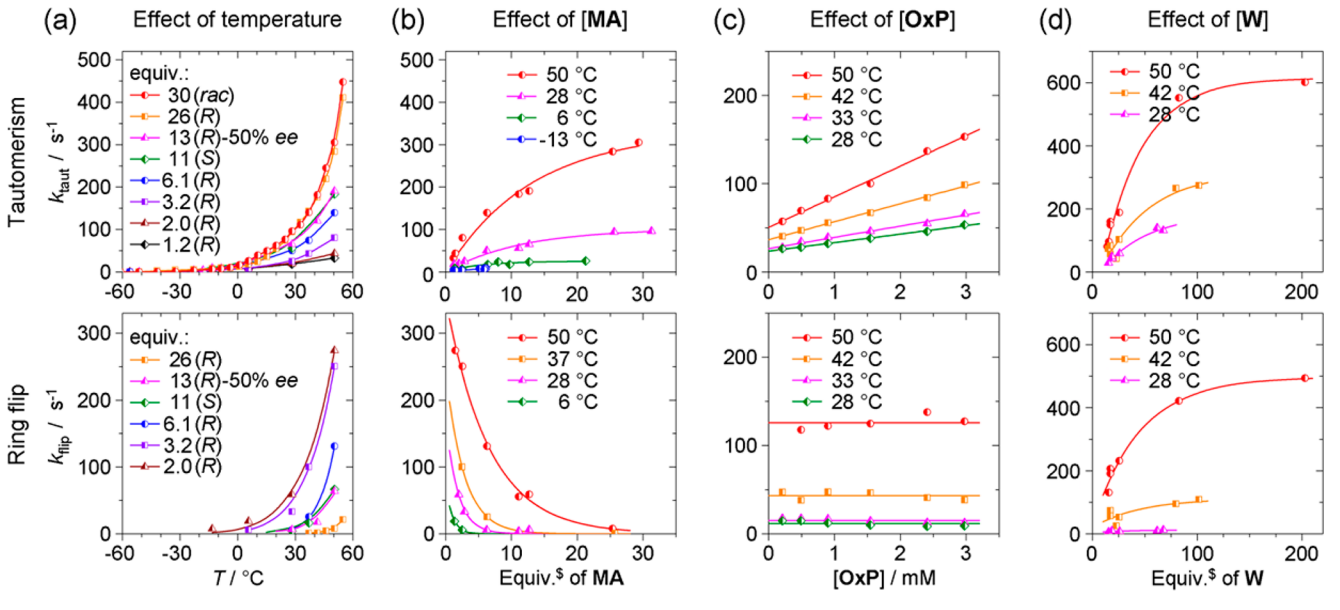

Figure 7. Dependencies of tautomerism rate k_{taut} (top panel) and ring-flip rate k_{flip} (bottom panel) values on various parameters: (a) temperature, (b) concentration of **MA**, (c) concentration of **OxP** and (d) concentration of water **W** as obtained from ^{1}H NMR fitting procedures. Details regarding composition of solutions: (a) Solution of **OxP** (ca. 1.8 mM, chloroform-*d*, ca. 20 equiv of **W**) with various **MA** concentrations. Temperature was varied. (b) Solution of **OxP** (1.8 mM, chloroform-*d*, ca. 20 equiv of **W**) with various (*R*)- or (*S*)-**MA** concentrations at different temperatures. Data were obtained from (a) using temperature−MA concentration transformation. (c) Solutions of **MA** (16.3 mM, chloroform-*d*, 50 mM of **W**) with various **OxP** concentrations at different temperatures. (d) Solution of **OxP** (2.5 mM, chloroform-*d*, ca. 5.8 equiv of **MA**) with various water **W** concentrations at different temperatures. Maximum solubility of **W** in chloroform-*d* was reached at each temperature. Symbol $ denotes number of equiv compared to **OxP** concentration.

dx.doi.org/10.1021/ja4124175 | J. Am. Chem. Soc. 2014, 136, 2112−2118

Increasing temperature increases the rate of ring-flip (Figure 7a, bottom panel) resulting in merging of the initially split resonances. ^{1}H NMR exchange spectroscopy (EXSY) at depressed temperature (−50 °C) contains no cross-peaks between the hemiquinonoid *ortho*-H, indicating that ring-flip has halted (Figure 6). With increasing temperature, however, the ratio between the volumes of cross-peaks and diagonal peaks increases, providing clear evidence of conformational exchange. Surprisingly, increasing the concentration of **MA** (at constant temperature) inhibits ring-flip as is manifested in NMR spectra in Figure 5b (by increasing splitting of resonances at 6.9 and 7.5 ppm) and is quantitatively plotted in Figure 7b. Note that rate of tautomerization concurrently increases. Thus, ring-flip and tautomerism have opposite rate dependencies on [**MA**]. This can be explained by variations in the equilibrium of species of **OxP** in the presence of **MA** as shown in Figure 8. Upon complexation (Figure 8a,b) two types

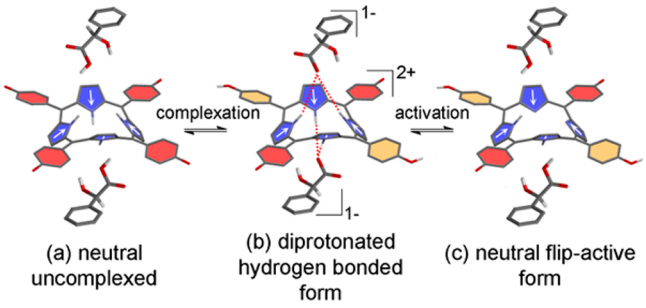

Figure 8. Equilibrium of **OxP** in the presence of **MA**. (a) Host−guest complexation. (b) Hydrogen-bonded flip-nonactive form (c) Possible ring-flip-active form.

of **OxP** are present in solution. A diprotonated, hydrogen-bonded form (Figure 8b) and a flip-active form (Figure 8c) capable of interconversion. At high concentrations of **MA**, the equilibrium shifts toward the diprotonated, hydrogen-bonded form, thus inhibiting ring-flip. In the flip-active form **OxP** bears two phenol groups, and the pyrrolic NH protons can exchange with carboxylic protons of **MA**. Activation enthalpy and entropy of tautomerism and ring-flip processes, respectively, can be calculated from Figures 7a using the Eyring equation, showing their increasing dependence on **MA** concentration, as seen in Figure S4.

The concentration of **OxP** itself (at constant temperature, [**MA**] and [**W**]) affects only the rate of tautomerism, while ring-flip is unaffected (Figure 7c). The tautomerism rate k_{taut} is linearly dependent on [**OxP**], suggesting that increasing concentration of **OxP** increases linearly collision frequency between **OxP** molecules (Figure S5) and thus enables proportionally faster intermolecular proton transfer. At infinite dilution ([**OxP**] → 0 in Figure 7c), it can be seen that rate of tautomerism is reduced but remains non-zero, which indicates the presence of intramolecular proton transfer. At higher concentrations of **OxP** (>2 mM), the intermolecular mechanism prevails (quantitative analysis can be found in Figure S6).

Water content increases the rates of both tautomerism and ring-flip significantly and serves as a mediator for both effects. Figure 7d illustrates how tautomerism and ring-flip in solutions of **OxP** and (*R*)-**MA** depend on water concentration. Extrapolation of k_{taut} to infinitely small water content ([**W**] → 0) suggests that water is essential for proton transfer within and between $\mathbf{OxPH_2}^{2+}$ molecules. Slower/faster ring-flip at lower/higher [**W**] might be associated with a situation where the equilibrium shown in Figure 8 is shifted toward the flip-non-active/flip-active form due to reduced/increased interaction of water with $\mathbf{OxPH_2}^{2+}$ and $\mathbf{MA}^-$ species, which enhance/obstruct formation of the hydrogen-bonded (flip-non-active) complex.

An interesting effect occurs in solutions of **OxP** and (*R*)-**MA** at low temperature (−56 °C), where interconversion between (+)-$\mathbf{OxPH_2}^{2+}$ and (−)-$\mathbf{OxPH_2}^{2+}$ enantiomers is suspended (see Figure 9a,b) due to zero rates of both tautomerism and ring-

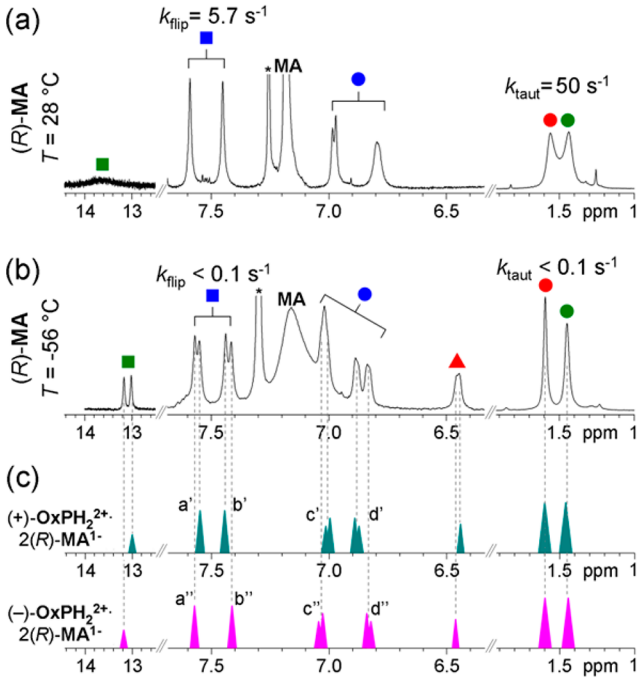

Figure 9. Differentiation of $\mathbf{OxPH_2}^{2+}$ enantiomers. ^{1}H NMR spectra of **OxP** (1.8 mM, chloroform-*d*) with 6.1 equiv of (*R*)-**MA** at (a) 28 °C (contain 15 equiv of **W**) and (b) −56 °C (contain 3.2 equiv of **W**), exhibiting additional splitting of most resonances due to formation of two diastereomers. For resonance assignment see Figure 3a. (c) Schematic assignment of spectrum to particular diastereomer based on NOESY (see Figure S7) and quantum mechanical calculations (see Figures S8−S10 and Data S1, S2, S3, and S4 for energy-minimized DFT structures of both diastereomers in two conformations calculated at ωB97XD/6-31G level of theory in IEFPCM).

flip. Additionally, the observed peak splitting can be attributed to two stable diastereomers formed in solution. (*R*)-**MA** here plays a role of chiral solvating agent and can differentiate the two $\mathbf{OxPH_2}^{2+}$ enantiomers, as seen in Figure 9b,c. In order to assign respective resonances to individual diastereomers, the low-temperature NOESY spectrum was measured (see Figure S7). Integration of the NMR spectrum (see region 6.9−6.8 ppm at −56 °C in Figure 9b, containing two resolved peaks for each diastereomer) indicates that both diastereomers have almost the same abundance (ratio (+)-$\mathbf{OxPH_2}^{2+}$·2(*R*)-$\mathbf{MA}^-$/(−)-$\mathbf{OxPH_2}^{2+}$·2(*R*)-$\mathbf{MA}^-$ is ca. 1.05).

The equilibrium between $\mathbf{OxPH_2}^{2+}$ enantiomers is dynamic at higher temperature, and the presence of (*R*)-**MA** and subsequent cooling might shift the abundance of diastereomers. Therefore, the similar abundances appear to be coincidental (a similar and contrasting examples can be seen for (*S*)-(+)-α-methoxyphenylacetic acid (Figure S11) and (*S*)-(−)-2-

dx.doi.org/10.1021/ja4124175 | J. Am. Chem. Soc. 2014, 136, 2112−2118

phenoxypropionic acid (Figure S12), respectively). Free energy differences between (+)-$\mathbf{OxPH_2}^{2+}$·2(*R*)-$\mathbf{MA}^-$ and (−)-$\mathbf{OxPH_2}^{2+}$·2(*R*)-$\mathbf{MA}^-$ diastereomers obtained from DFT calculation are relatively small (0.3 kcal/mol), supporting their equal abundance. Moreover, ^{1}H NMR spectra were also calculated (see Figure S9), allowing connection of each diastereomer to its measured spectrum, as seen in Figure 9b,c.

Molecular dynamics (MD) simulations (for details see Methods of MD in SI) were performed on both diastereomeric complexes at 25 °C. The vector which defines mutual direction between $\mathbf{MA}^-$ and $\mathbf{OxPH_2}^{2+}$ was introduced (see Methods of MD in SI), and its time-dependent projection on the mean $\mathbf{OxPH_2}^{2+}$ plane (using polar φ coordinate) was recorded. Consequently, the probability density function, $\rho(\varphi)$, describing preferences in mutual host−guest orientations, was constructed. $\rho(\varphi)$ of both diastereomers is shown in Figure 10. A distinct difference between $\rho(\varphi)$ of (+)-$\mathbf{OxPH_2}^{2+}$·2(*R*)-$\mathbf{MA}^-$ and (−)-$\mathbf{OxPH_2}^{2+}$·2(*R*)-$\mathbf{MA}^-$ diastereomers can be observed. This difference supports the observed additional split in ^{1}H NMR spectrum (at low temperature), as depicted in Figures 9b,c.

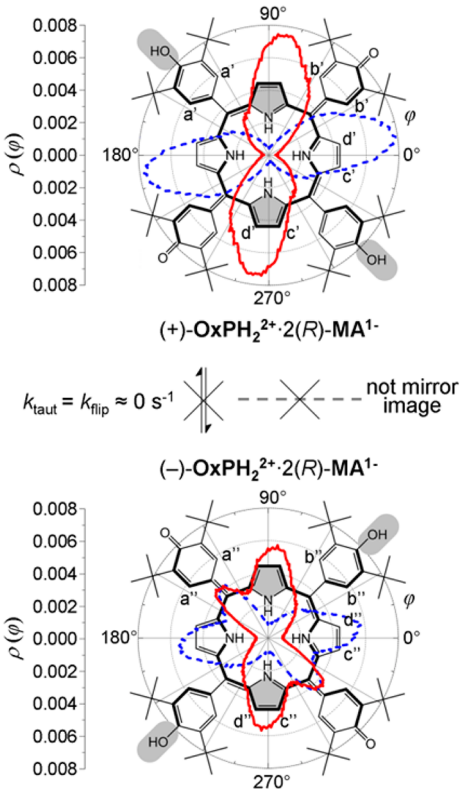

Figure 10. Structures of diastereomers. The (*R*)-**MA** guest is represented as probability density function $\rho(\varphi)$ ("chiral field") as obtained from MD simulations. Red line and dashed blue line denote guest (*R*)-**MA** molecule above and below host, respectively.

CONCLUSIONS

In summary, we report the use of a chiral reagent to investigate the binding properties, prototropic tautomerism, and saddle-to-saddle macrocyclic inversion (ring-flip) in the diprotonated form of **OxP**. Use of a chiral probe is an essential feature, since ring-flip processes would be otherwise unobservable. Both intra- and (predominantly) intermolecular proton transfer (tautomerism) were shown to occur. Tautomerism and ring-flip have been effectively deconvoluted and appear to be independent processes, which can be influenced or triggered (to some extent independently) by varying temperature or concentrations of the **OxP**, **MA**, and **W** reagents. Unexpectedly, we observed that increasing the concentration of **MA** leads to suppression of the ring-flip. Moreover, the presence of water, which is usually neglected or considered an impurity, has a significant influence on dynamics in this system. The diprotonated form of **OxP** exhibits dynamic interconversion (racemization) between two enantiomeric forms through both tautomerism and ring-flip mechanisms. At depressed temperature, interconversion can be arrested, and the ratio between enantiomers can be altered, depending on the identity of the protonating agent ((*R*)-**MA**, (*S*)-(−)-2-phenoxypropionic acid, etc.). Our observations imply that reactivity of functional groups in molecules undergoing tautomerism (or ring-flip) can be significantly altered, leading to different yields of respective products during (e.g., asymmetric) syntheses based on solution properties, including reagent concentrations and impurities such as water.

EXPERIMENTAL SECTION

OxP was prepared by a previously reported method.[21−23] (*R*)-**MA** and (*S*)-**MA**, (*S*)-(−)-2-phenoxypropionic acid, (*rac*)-(−)-2-phenoxypropionic acid (Wako Chem. Co.), and (*S*)-(+)-α-methoxyphenylacetic acid (TCI Co. Ltd.) were used as received. Chloroform-*d* used for ^{1}H NMR spectroscopy was obtained from Cambridge Isotope Ltd. Water used for titrations was distilled using an Autostill WG220 (Yamato) and deionized using a Milli-Q Lab (Millipore). ^{1}H NMR spectra were recorded using an AL300BX (JEOL) spectrometer operating at 300.4 MHz (unless stated otherwise). DFT ωB97XD[31] functional with 6-31G basis set and IEFPCM (ε = 4.71) implemented in Gaussian 09[32] was used for quantum mechanical calculations. Amber 11[33] simulation package with GAFF[34] parameters and RESP charges[35] was used for classical molecular dynamics simulations.

ASSOCIATED CONTENT

Supporting Information

Additional details concerning sample preparation, experimental procedures, derivation of host−guest binding model, fitting of two-site symmetrical exchange spin system, DFT calculations, classical molecular dynamics simulations, 2D NMR spectra of **OxP**/**MA** system, and additional results for two other acids (guests). This material is available free of charge via the Internet at http://pubs.acs.org.

AUTHOR INFORMATION

Corresponding Authors

labuta.jan@nims.go.jp
jonathan.hill@nims.go.jp

Notes

The authors declare no competing financial interest.

ACKNOWLEDGMENTS

This work was partly supported by World Premier International Research Initiative (WPI Initiative), MEXT, Japan, and Core Research for Evolutional Science and Technology (CREST) and Precursory Research for Embryonic Science and Technology (PRESTO) both of Japan Science and Technology Agency (JST), Japan.

REFERENCES

(1) Stone, A.; Fleischer, E. B. *J. Am. Chem. Soc.* **1968**, *90*, 2735−2748.
(2) Cheng, B.; Munro, O. Q.; Marques, H. M.; Scheidt, W. R. *J. Am. Chem. Soc.* **1997**, *119*, 10732−10742.
(3) Rayati, S.; Zakavi, S.; Ghaemi, A.; Carroll, P. J. *Tetrahedron Lett.* **2008**, *49*, 664−667.
(4) Labuta, J.; Ishihara, S.; Shundo, A.; Arai, S.; Takeoka, S.; Ariga, K.; Hill, J. P. *Chem.—Eur. J.* **2011**, *17*, 3558−3561.
(5) Barkigia, K. M.; Berber, M. D.; Fajer, J.; Medforth, C. J.; Renner, M. W.; Smith, K. M. *J. Am. Chem. Soc.* **1990**, *112*, 8851−8857.
(6) Nurco, D. J.; Medforth, C. J.; Forsyth, T. P.; Olmstead, M. M.; Smith, K. M. *J. Am. Chem. Soc.* **1996**, *118*, 10918−10919.
(7) Shundo, A.; Labuta, J.; Hill, J. P.; Ishihara, S.; Ariga, K. *J. Am. Chem. Soc.* **2009**, *131*, 9494−9495.
(8) Labuta, J.; Ishihara, S.; Šikorský, T.; Futera, Z.; Shundo, A.; Hanyková, L.; Burda, J. V.; Ariga, K.; Hill, J. P. *Nat. Commun.* **2013**, *4*, 2188.
(9) Mizuno, Y.; Aida, T.; Yamaguchi, K. *J. Am. Chem. Soc.* **2000**, *122*, 5278−5285.
(10) Hill, J. P.; Schumacher, A. L.; D'Souza, F.; Labuta, J.; Redshaw, C.; Elsegood, M. R. J.; Aoyagi, M.; Nakanishi, T.; Ariga, K. *Inorg. Chem.* **2006**, *45*, 8288−8296.
(11) Rambo, B. M.; Sessler, J. L. *Chem.—Eur. J.* **2011**, *17*, 4946−4959.
(12) Hargrove, A. E.; Nieto, S.; Zhang, T.; Sessler, J. L.; Anslyn, E. V. *Chem. Rev.* **2011**, *111*, 6603−6782.
(13) Ishihara, S.; Labuta, J.; Šikorský, T.; Burda, J. V.; Okamoto, N.; Abe, H.; Ariga, K.; Hill, J. P. *Chem. Commun.* **2012**, *48*, 3933−3935.
(14) Shundo, A.; Ishihara, S.; Labuta, J.; Onuma, Y.; Sakai, H.; Abe, M.; Ariga, K.; Hill, J. P. *Chem. Commun.* **2013**, *49*, 6870−6872.
(15) Ishihara, S.; Iyi, N.; Labuta, J.; Deguchi, K.; Ohki, S.; Tansho, M.; Shimizu, T.; Yamauchi, Y.; Sahoo, P.; Naito, M.; Abe, H.; Hill, J. P.; Ariga, K. *ACS Appl. Mater. Interfaces* **2013**, *5*, 5927−5930.
(16) Ishihara, S.; Hill, J. P.; Shundo, A.; Richards, G. J.; Labuta, J.; Ohkubo, K.; Fukuzumi, S.; Sato, A.; Elsegood, M. R. J.; Teat, S. J.; Ariga, K. *J. Am. Chem. Soc.* **2011**, *133*, 16119−16126.
(17) Furusho, Y.; Kimura, T.; Mizuno, Y.; Aida, T. *J. Am. Chem. Soc.* **1997**, *119*, 5267−5268.
(18) Hembury, G. A.; Borovkov, V. V.; Inoue, Y. *Chem. Rev.* **2008**, *108*, 1−73.
(19) Toyofuku, K.; Alam, M. A.; Tsuda, A.; Fujita, N.; Sakamoto, S.; Yamaguchi, K.; Aida, T. *Angew. Chem., Int. Ed.* **2007**, *46*, 6476−6480.
(20) Micali, N.; Engelkamp, H.; van Rhee, P. G.; Christianen, P. C. M.; Monsù Scolaro, L.; Maan, J. C. *Nature Chem.* **2012**, *4*, 201−207.
(21) Milgrom, L. R. *Tetrahedron* **1983**, *39*, 3895−3898.
(22) Hill, J. P.; Hewitt, I. J.; Anson, C. E.; Powell, A. K.; McCarty, A. L.; Karr, P. A.; Zandler, M. E.; D'Souza, F. *J. Org. Chem.* **2004**, *69*, 5861−5869.
(23) Hill, J. P.; Schmitt, W.; McCarty, A. L.; Ariga, K.; D'Souza, F. *Eur. J. Org. Chem.* **2005**, 2893−2902.
(24) Storm, C. B.; Teklu, Y. *J. Am. Chem. Soc.* **1972**, *94*, 1745−1747.
(25) Schlabach, M.; Rumpel, H.; Limbach, H.-H. *Angew. Chem., Int. Ed. Engl.* **1989**, *28*, 76−79.
(26) The type (sign) of (+)- and/or (−)-enantiomer of $\mathbf{OxPH_2}^{2+}$ was chosen arbitrarily and is kept consistent throughout this article. The structures of both enantiomers are shown in Figure 2.
(27) Connors, K. A.; Paulson, A.; Toledo-Velasquez, D. *J. Org. Chem.* **1988**, *53*, 2023−2026.
(28) Walter, R. I.; Ojadi, E. C. A.; Linschitz, H. *J. Am. Chem. Soc.* **1993**, *97*, 13308−13312.
(29) Římal, V.; Štěpánková, H.; Štěpánek, J. *Concepts Magn. Reson. Part A* **2011**, *38*, 117−127.
(30) Alexander, S. *J. Chem. Phys.* **1962**, *37*, 967−974.
(31) Chai, J.-D.; Head-Gordon, M. *Phys. Chem. Chem. Phys.* **2008**, *10*, 6615−6620.
(32) Frisch, M. J.; Trucks, G. W.; Schlegel, H. B.; Scuseria, G. E.; Robb, M. A.; Cheeseman, J. R.; Scalmani, G.; Barone, V.; Mennucci, B.; Petersson, G. A.; Nakatsuji, H.; Caricato, M.; Li, X.; Hratchian, H. P.; Izmaylov, A. F.; Bloino, J.; Zheng, G.; Sonnenberg, J. L.; Hada, M.; Ehara, M.; Toyota, K.; Fukuda, R.; Hasegawa, J.; Ishida, M.; Nakajima, T.; Honda, Y.; Kitao, O.; Nakai, H.; Vreven, T.; Montgomery, J. A., Jr.; Peralta, J. E.; Ogliaro, F.; Bearpark, M.; Heyd, J. J.; Brothers, E.; Kudin, K. N.; Staroverov, V. N.; Kobayashi, R.; Normand, J.; Raghavachari, K.; Rendell, A.; Burant, J. C.; Iyengar, S. S.; Tomasi, J.; Cossi, M.; Rega, H.; Millam, J. M.; Klene, M.; Knox, J. E.; Cross, J. B.; Bakken, V.; Adamo, C.; Jaramillo, J.; Gomperts, R.; Stratmann, R. E.; Yazyev, O.; Austin, A. J.; Cammi, R.; Pomelli, C.; Ochterski, J. W.; Martin, R. L.; Morokuma, K.; Zakrzewski, V. G.; Voth, G. A.; Salvador, P.; Dannenberg, J. J.; Dapprich, S.; Daniels, A. D.; Ö. Farkas, Foresman, J. B.; Ortiz, J. V.; Cioslowski, J.; Fox, D. J. *Gaussian 09*, Revision A.1; Gaussian, Inc.: Wallingford, CT, 2010.
(33) Case, D. A.; Darden, T. A.; Cheatham, T. E.; Simmerling, C. L.; Wang, J.; Duke, R. E.; Luo, R.; Walker, R. C.; Zhang, W.; Merz, K. M.; Roberts, B.; Wang, B.; Hayik, S.; Roitberg, A.; Seabra, G.; Kolossvary, I.; Wong, K. F.; Paesani, F.; Vanicek, J.; Liu, J.; Wu, X.; Brozell, S.; Steinbrecher, T.; Gohlke, H.; Cai, Q.; Ye, X.; Wang, J.; Hsieh, M.-J.; Cui, G.; Roe, D. R.; Mathews, D. H.; Seetin, M. G.; Sagui, C.; Babin, V.; Luchko, T.; Gusarov, S.; Kovalenko, A.; Kollman, P. A. Amber 11; University of California: San Francisco, 2010.
(34) Wang, J.; Wolf, R. M.; Caldwell, J. W.; Kollman, P. A.; Case, D. A. *J. Comput. Chem.* **2004**, *25*, 1157−1174.
(35) Bayly, C. I.; Cieplak, P.; Cornell, W.; Kollman, P. A. *J. Phys. Chem.* **1993**, *97*, 10269−10280.